Delft University of Technology

BSc Thesis

Performed at:
Department of Acoustic Wavefield Imaging
Faculty of Applied Sciences

Null subtraction imaging for small aperture phased array transducers

Author:
V.W.J. Heusinkveld

Supervisor:
Dr. Ir. M. D. Verweij

Graduation Committee:
Prof. Dr. Ir. N. de Jong
Dr. Ir. M. D. Verweij
Dr. N. Bhattacharya
Dr. V. Daeichin

Delft
July 12, 2017

Abstract

In medical ultrasound imaging phased array transducers are used for non-invasive imaging. However, for 3D intra-cardiac-echography technical borders are reached since blood vessel size limits the dimensions of the array. This dimensional limitation lowers lateral resolution. To solve part of the problem, unconventional ways of improving lateral resolution are needed.

For linear arrays Reeg [1] proposed null subtraction imaging (NSI), which resulted at best in 30 dB lower side lobes and a beamwidth reduction of up to 25 times. This is a non-linear image processing technique based on implementing multiple apodizations in post-processing. Within this method three images are made of which one has a sharp drop to zero in the middle which can be exploited by subtracting it from the other images. This results in an improvement over a regular apodization scheme.

To verify the technique for 2D phased array imaging, simulations are done using Field-II [2, 3] while taking array dimension into account. Measurements take place on an artificial phantom with evenly spaced line scatter targets. For the experiment a P4-l phased array transducer is used in combination with a Verasonics Vantage 256$^{\text{TM}}$where a sub-aperture of 30 elements is chosen. The experiment is done on a CIRS 040GSE phantom, where evenly spaced line scatter targets and tightly spaced lateral resolution targets are looked at. To form an image a simple delay-and-sum (DAS) algorithm is used. The effect of NSI on the speckle in an image is also measured, where for normal developed speckle a signal to noise ratio (SNR) of 1.91 is expected.

Results for simulation are as expected with an average beamwidth reduction of 22.5 times and an on average higher main lobe to side lobe ratio (MSR) of 33.4 dB for NSI imaging, opposed to using a rectangular apodization. Experimentally, an average beamwidth reduction of 5 times and an on average higher MSR of 20.5 dB are realised. The beamwidth reduction is lower than expected. This is due to rounding errors in the DAS algorithm, were data can only be delayed by integer elements.

For the tightly spaced lateral scatter targets no extra targets can be distinguished when using NSI imaging opposed to rectangular apodization imaging, only the targets that where already visible show reduction in beamwidth and side lobe levels.

When using NSI speckle SNR is reduced from 1.78 to on average 0.50 and seems to scale with energy present in the image. A hybrid image between the NSI image and rectangular apodization image is made to overcome this reduction in speckle SNR. It results in reduced beamwidth, restores speckle SNR but increases side lobe levels.

It can be concluded that the NSI method works for phased array imaging under perfect conditions, the simulation. To achieve the full potential of the technique more research is needed regarding the effects of improper sampling. This led to less than ideal 'sharp' drops during the experiment, lowering the reduction in beamwidth. Also, the reduced speckle needs further research to understand its behaviour. Once these things are achieved the next step to 3D imaging can be made.

Acknowledgements

First of all, I would like to thank my supervisor Martin Verweij. He was always open to questions, provided me with feedback and guided me throughout the whole process. This all helped a lot in exploring this, for me, partly new field in Physics. Secondly, I would like to thank Verya Daeichin for helping me during the experimental part of my research and providing me with helpful insights and discussion. Lastly, I would like to thank Delft University of Technology for providing me with highend equipment and a challenging environment to conduct research.

Contents

1. Introduction

In the medical field ultrasound imaging using transducers is used as a non-invasive imaging method. The transducers are made up of piëzo electric elements in array form, which have the ability to transform electric charge into pressure and vice versa. This characteristic can be used to send and receive pressure fields with high frequencies (typically greater than 20 kHz). In general, a transducer makes contact with the skin using a certain gel which transfers the energy of the pressure field to the inside of the body. In other cases, for example during heart surgery, a transducer is brought into the heart. This intra-cardiac echography (ICE) is currently limited to 2D imaging.

To make ultrasound images, the imaging plane is divided into hundreds of scan lines. Depending on the method, phased or linear array imaging, the plane is scanned under different angles or linearly. Per line a focused beam is sent out by a 1D transducer array. The different kinds of tissue that are in the path of the pressure field scatter and reflect this field. Some of it gets detected by the transducer yielding the raw non-beamformed data. In conventional B-mode imaging this raw data gets processed using a delay-and-sum (DAS) algorithm and gets envelope-detected by taking the absolute value of the analytic signal. These beam formed scan lines can be plotted to form the image.

The next step in ICE will be 3D imaging, for which a 2D array is needed. A limiting factor is a maximum array size of approximately 3 mm, which is small compared to traditional array sizes. This gives rise to problems, among other things, the lateral resolution of the resulting image [4]. This thesis tries to tackle a part of this problem utilizing the null subtraction imaging method (NSI), first introduced [1] and later patented [5] by R. Reeg, which promises a reduction in beamwidth of up to 25 times for linear transducer arrays.

NSI is based on the weights the different array elements get in receive, the so called apodization. In general when dealing with a single rectangular apodization window, the point spread function will look like a sinc function with side lobe levels at around -13 dB relative to the top (without using any focus on transmit). The width of the main lobe is limited by the diffraction limit. For NSI three images are generated, one for which the apodization is chosen such that there is a sharp null centered in between the two side lobes and two to form a image for which there is a 'bridge' in between the side lobes. These images are subtracted to get an image with lower side lobe levels and reduced main lobe width.

The goal of this thesis is to develop and validate this method for phased array imaging and determine the improvement over a standard rectangular apodization. This is done for a 1D array, first using simulation where the spatial dimensions of the 3D-ICE are taken into account, and afterwards in a real world experiment using the Verasonics with an existing phased array used in general echography.

This thesis is part of the Bachelor End Project (BEP) done at the Acoustic Wavefield Imaging research group (AWI) of Delft University of Technology.

2. Theory

2.1 Imaging

2.1.1 Array types

In general there are two types of transducer arrays that are used in ultrasound imaging. First there is the linear array transducer, in which the data acquisition is done as follows. From the total array a sub-array is chosen, often much smaller than the array itself. This sub-array can then be used to scan a line perpendicular to the array at different distances (focus in transmission). After the data has been stored the whole sub array shifts one element and the whole process starts again, until the last element of the array is reached. This process is illustrated in figure 2.1. After a whole area is scanned the data can be further processed to form an image as explained later in section 2.1.2.

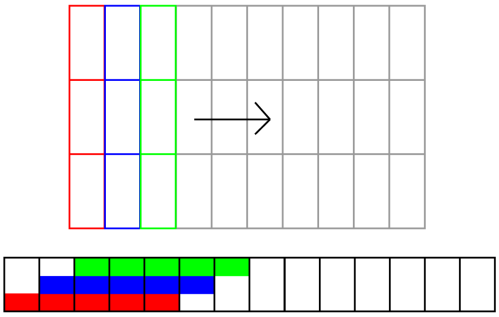

Figure 2.1: Illustration of linear array imaging. The bottom array represents the transducer, the matrix represents the scanned area at a certain depth. The colour indicates with what sub-array a line is scanned for the first three acquisitions.

Second, there is the phased array. The process has a lot of similarity to the linear array but instead of a perpendicular scan line, the scan line is steered under an angle, as illustrated in figure 2.2. This steering is realised by delaying the traducer elements in such a way that a wave seems to leave the transducer surface under an angle. After one such line is acquired the angle is incremented until the desired area is scanned. The advantage of this technique is that with a relatively small array a big area or volume can be scanned. Again, after all the data is gathered an image can be made.

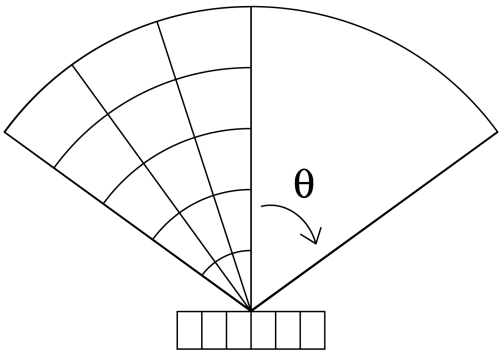

Figure 2.2: Illustration of phased array imaging. Here θ is the angle under which the beam is steered.

2.1.2 Beam forming

To form an image out of the raw data, it first needs to be beamformed which can be done using a delay-and-sum (DAS) algorithm. After DAS the signal needs to be envelope-detected, a method to do this is by taking the absolute value of the analytic signal [6].

Delay-and-sum

In essence, this means that the individual array elements are delayed in such a way that an artificial focus point is created. Since the main aspect in this thesis considers phased arrays without focussing on transmission, so only steering, we look at the algorithm for focussing in receive [7]. If the elements are defined as in Figure 2.3,

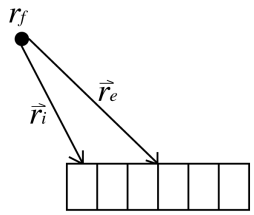

Figure 2.3: The focus point r_f, $\vec{r}_e$ the distance to a receiving element, $\vec{r}_i$ the distance to the center of the array.

then the relative delays are given as:

$$\tau(i) = \frac{|\vec{r}_e| - |\vec{r}_i|}{c} \tag{2.1}$$

with c as the speed of sound in the given medium and $\tau(i)$ as the delay to the corresponding element. After the respective signals are delayed accordingly they can be summed to give the radiation pattern at and near the focus point.

Envelope detection

The envelope of a signal is defined as the magnitude of the analytic signal [8],

$$Env(x(t)) = \sqrt{(x(t))^2 + (H[x(t)])^2} \tag{2.2}$$

where H repents the Hilbert transform and x the signal that gets envelope-detected. The result of envelope detection is shown in figure 2.4. After envelope detection the data can be plotted to form the image.

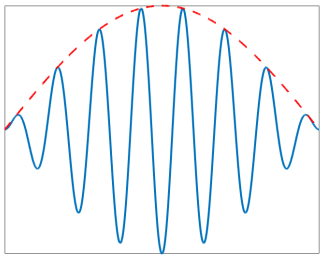

Figure 2.4: Illustration of what envelope detection does. The solid line is the signal that gets envelope detected and the dashed line is the envelope-detected signal.

2.1.3 Lateral resolution

The lateral resolution gets determined by the width of the beam at -6 dB relative to the top (this is half of the maximum). When a standard rectangular transducer window is used, so all elements get excited with the same weight, this so called full width half maximum is defined as [6]:

$$\text{FWHM} = 1.206\lambda\frac{F}{L} \tag{2.3}$$

where λ is the wavelength of the center frequency of the transducer, F the distance from the transducer and L aperture size.

2.1.4 The far field

It is only appropriate to use the term far field for a non focussed beam [6]. It is defined as follows:

$$S = \frac{L^2}{4\lambda} \tag{2.4}$$

where S is the distance to the transducer from which on the far field starts. For the method used, as explained later, it is important that measurements take place in this zone.

2.2 The NSI method

The NSI method of Reeg is based on the following theory [1]. The far field beam pattern is proportional to the absolute Fourier transform of the field at the originating plane as can be seen from the Fresnel approximation [6]. For a transducer this field is determined by the product of the apodization and the aperture. When both are chosen rectangular the Fourier transform results in a sinc (the fourier transform of a rectangular function), as can be seen in figure 2.5a. Using Fourier transform pairs an apodization can be found (figure 2.5b) that results in a sharp null in the middle of the Fourier transform (figure 2.5d). For the transforms see appendix A.1.

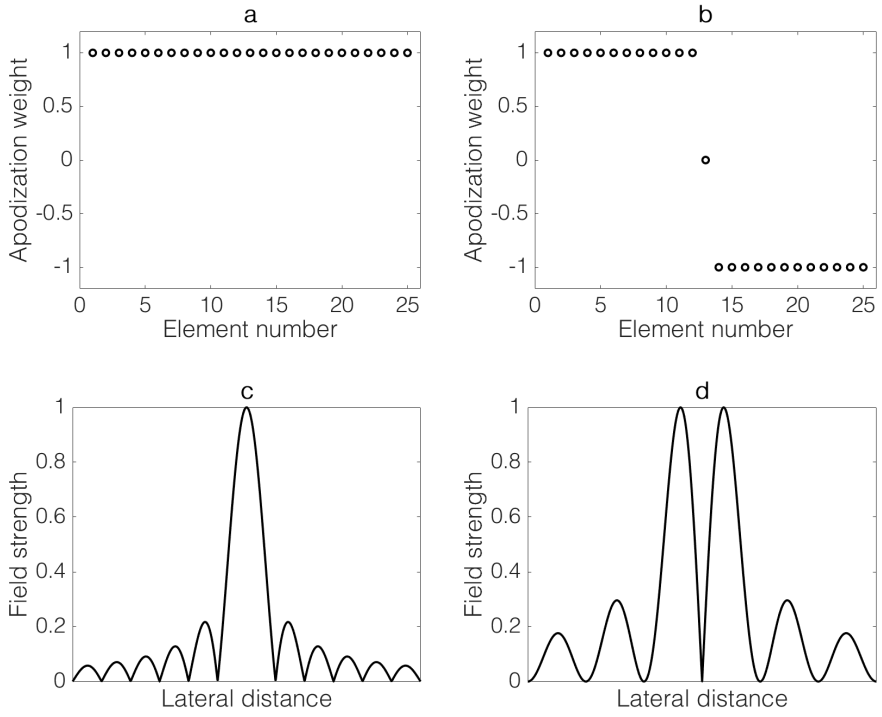

Figure 2.5: Apodization functions and their respective radiation patterns. (a) A rectangular apodization in which all the elements are equally weighed. (b) A zero-mean apodization in which all elements are equally weighted although half with a minus sign, and in case of an odd number of elements a null in the middle. (c) Corresponding radiation pattern to (a). (d) Corresponding radiation pattern to (b) with sharp drop to in the middle.

The behaviour is as expected with a wide main lobe restricted by diffraction limits and smaller side lobes (figure 2.5c). The field that is created by the zero-mean apodization has a sharp drop to zero in the middle, the exploitation of this property forms the basis of the NSI technique. To achieve this one cannot simply invert the image since the resulting side lobe levels are as high as main lobe levels as can be seen in figure 2.6a. Also subtracting a constant times 2.5d from 2.5c does not result in an improvement since it gives rise to a radiation pattern as shown in figure 2.6b, where the main lobe is marginally less wide.

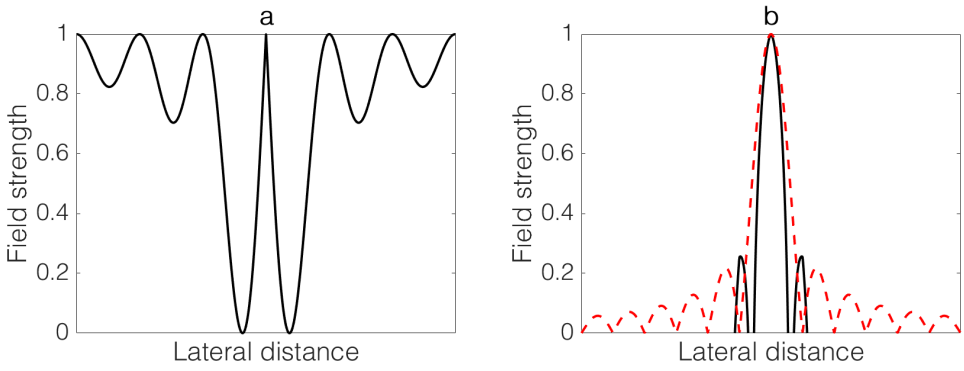

Figure 2.6: Resulting radiation patterns of possible subtraction techniques. (a) Inverted zero-mean apodization radiation pattern, sharp main lobe with high side lobe levels. (b) The resulting radiation pattern from subtracting the zero-mean apodization image from the rectangular apodization image (solid line). The dashed line is the original radiation pattern from rectangular apodization.

The bridging approach

To overcome these problems the following approach is taken, called the "bridging" approach [1]. For this method, first an image is constructed using the zero-mean apodization, in formula form for a even number of elements N:

$$Apo_{zm}(i) = \begin{cases} 1 & \text{if} \quad 1 < i \leq \frac{N}{2} \\ -1 & \text{if} \quad \frac{N}{2} < i \leq N \end{cases} \tag{2.5}$$

and for odd N:

$$Apo_{zm}(i) = \begin{cases} 1 & \text{if} \quad 1 < i \leq floor(\frac{N}{2}) \\ 0 & \text{if} \quad i = ceil(\frac{N}{2}) \\ -1 & \text{if} \quad ceil(\frac{N}{2}+1) \leq i \leq N \end{cases} \tag{2.6}$$

where i is the element number (integer), floor rounds to the nearest integer towards minus infinity and ceil rounds to the nearest integer towards plus infinity. Now two new apodizations are defined. The first by adding a small constant to the apodization:

$$Apo_{zmc} = Apo_{zm} + c \tag{2.7}$$

and the second by mirroring the zero-mean apodization in its center and adding the same constant:

$$Apo_{zmcm} = -Apo_{zm} + c \tag{2.8}$$

this constant is small opposed to the original apodization as will be elaborated on later. Both datasets from Apo_{zmc} and Apo_{zmcm} are delay-and-summed, envelope-taken and added together after which they are normalized to from a new image. This results in an almost identical image to the zero-mean apodization apart from a non-zero "bridge" connecting the two side lobes, where the constant determines the amount of bridging. This is illustrated in figure 2.7. As can be seen, a bridging constant that is around a tenth of the original apodization should give adequate bridging.

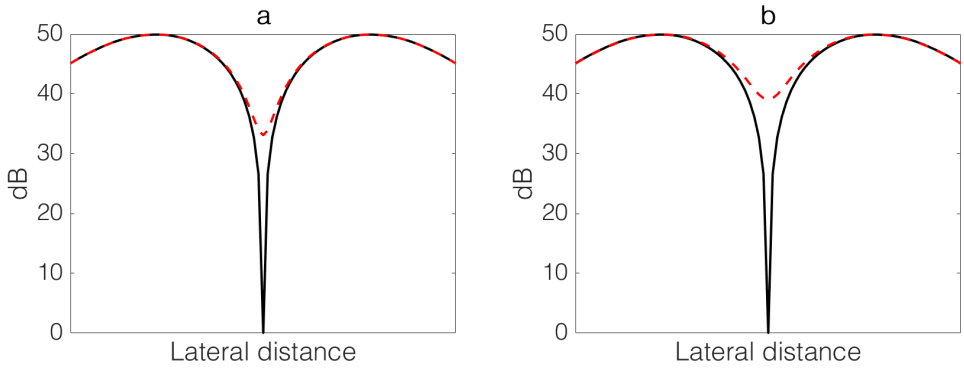

Figure 2.7: Radiation patterns, for the solid line the zero-mean apodization is used and for the dashed line the bridging apodization scheme is used. This is done for different constants in formula 2.7 and 2.8. (a) c = 0.1. (b) c = 0.2.

When the zero-mean apodization image is subtracted from the bridged image, resulting in the NSI image, a radiation pattern as in figure 2.8 can be expected. Resulting in a much narrower main lobe and lower side lobes as favoured.

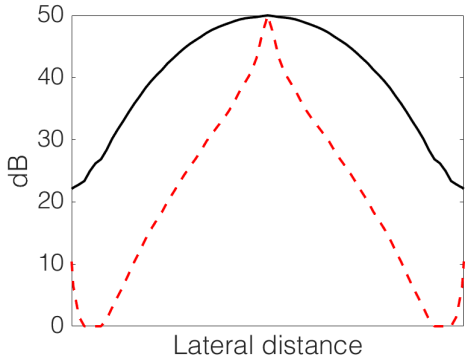

Figure 2.8: Dashed line, expected radiation pattern using the NSI apodization scheme. Solid line, expected radiation pattern using rectangular apodization.

3. Verification

For this verification first a simulation is done in Field-II [2, 3] to verify the method for phased array imaging. Afterwards and experiment is performed using a traditional transducer to determine the real world performance.

3.1 Simulation

3.1.1 Setup specifications

Based on the transducer proposed in [4] the following specifications are used. The transducer is 1D, 3 mm in width and consists of 25 elements. The pitch, the distance from center to center, is chosen to be 120 μm and the individual elements 100 μm in width which results in a 20 μm kerf, the distance between the elements. The center frequency of the phased array is 7.5 MHz.

The virtual phantom on which the experiment will take place consists of three line scatter targets at a depth of respectively 20, 40 60, and 80 mm. This is done to show the effectiveness of NSI at the different depths that are in the foreseen region for the application of this phased array [4].

3.1.2 Simulation settings

As mentioned before, the simulation is done using the Field-II program, which consists a library of MATLAB functions while it does most of its computations in a program written in C. This results in relatively fast simulations.

The specifications of the transducer array are put in. Instead of the suggested sampling frequency of 30 MHz, mentioned in the research proposal, a sampling frequency of 100 MHz is used. This is done to show what the technique is able to achieve without being limited to the sampling frequency. The speed of sound in tissue is set to the standard 1540 m/s. For the impulse response of the elements a two-period sine function multiplied by a Gaussian window [9] is used. Ideally this would give an impulse response as in figure 3.1a but due to the sampling frequency it will lead to the impulse response like figure 3.1b. Which shows that 100 MHz is a good sampling rate.

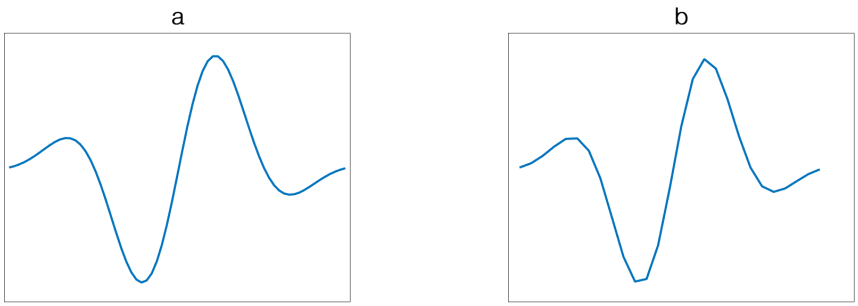

Figure 3.1: Impulse response of a simulated transducer element. (a) The ideal impulse response. (b) Impulse response under sampling frequency of 100 MHz.

3.1.3 Data acquisition

During transmit and receive all the 25 elements are used. In transmit a plane wave is used, this is done to demonstrate the abilities of the technique in post-processing. The plane wave is generated by putting the artificial focal point at infinity, leaving only the natural focus of the transducer. This wave is steered 500 times in a sector reaching form -30 to 30 degrees, where the sector is divided up in to 500 scan lines to have a proper resolution ($\approx$ 0.17 mm per scan line at 8 cm depth). For every transmission the corresponding received signal is stored. To get this data from individual elements the calc_scat_multi() function from Field can be used [10]. This function also returns the time it took the first receive signal to be registered, this can later be used to adjust the data in time.

3.1.4 Data processing

Now we are left with all the raw data which consists of 500 lines, each received with 25 elements. First the data needs to be beam formed. For this the DAS algorithm is used as explained earlier. The data gets delayed as given in formula 2.1. To apply the NSI technique, three summations need to be made plus one summation for the original image as a comparison.

For the original image a square apodization is used, so all elements are summed with weight 1. For the NSI image a zero-mean apodization is needed so the data is summed with weights as given in formula 2.6. This summation is also done for the zero-mean plus constant apodization and the mirror of that as by formula 2.7 and 2.8, where the constant is taken to be 0.05, 0.1 and 0.2 respectively to research the effect.

Afterwards all individual data sets get adjusted in time, with the information from the calc_scat_multi() function, and envelope detected using the hilbert() function of MATLAB, which returns the discrete analytical function, and taken absolute.

To form a reference image the data with the rectangular apodization gets logarithmically compressed to a 50 dB dynamic range. For the NSI image first the zero-mean plus constant and the mirror apodization data needs to be added together with weights 0.5 to form the bridged data. To get the NSI data the zero-mean apodization data needs to be subtracted from the bridged data. After which the NSI data gets the same logarithmic compression as the original image. In appendix A.2 a graphical overview of the procedure is added.

To compare the NSI technique to the original image the lateral resolution improvement at -6 dB from the top (the beamwidth) and the main lobe to side lobe ratio (MSR) are estimated at the four different depths of the line scatter targets. This is done with a 80 dB dynamic range as otherwise side lobes would not be visible in some cases. Based on the paper of Reeg an MSR improvement of 30 dB can be expected and a beamwidth improvement of 10 to 25 times [1].

3.2 Experiment

The real world experiment will be done using a Verasonics Vantage 256^{TM} in combination with a P4-1 transducer. The Verasonics, which has the ability to serve 256 transmit and receive channels, acts like a bridge between the computer and the transducer. The full set-up can be seen in Figure 3.2.

Figure 3.2: Experimental set-up. On the left the CIRS phantom can be seen with on top of it the P4-1 transducer. In the middle is the Verasonics and on the right the PC to which it is connected.

3.2.1 Setup specifications

The P4-1 is a phased array transducer consisting of 96 elements and has a center frequency of 2.5 MHz. The elements have a width of 0.245 mm and a kerf of 0.05 mm resulting in a total transducer width of 28.32 mm, which is an order bigger than the simulated array. Using formula 2.4, it can be determined that the far field starts at 30 cm for an unfocussed beam. Since that is too far for this experiment a sub-aperture of 30 elements is chosen, resulting in a width of 8.85 mm and bringing the far field back to 3 cm. This is done as a demonstration and not to test 3D-ICE since transducer specifications do not match.

Measurements will take place on a CIRS phantom (model 040GSE), where a schematic of the inside is shown in Figure 3.3a and an image in Figure 3.3b. The background 'noise' that can be seen in figure 3.3b is called speckle, which is important because it shows anechoic areas. For this experiment it is most interesting to look at the lateral resolution region of the phantom, indicated with red (dark) box in the figure. That is because the technique aims to improve this resolution. The line scatterers, indicated by the blue (light) box, will also be imaged, since they give a nice view of the point spread function at different depths.

(a)

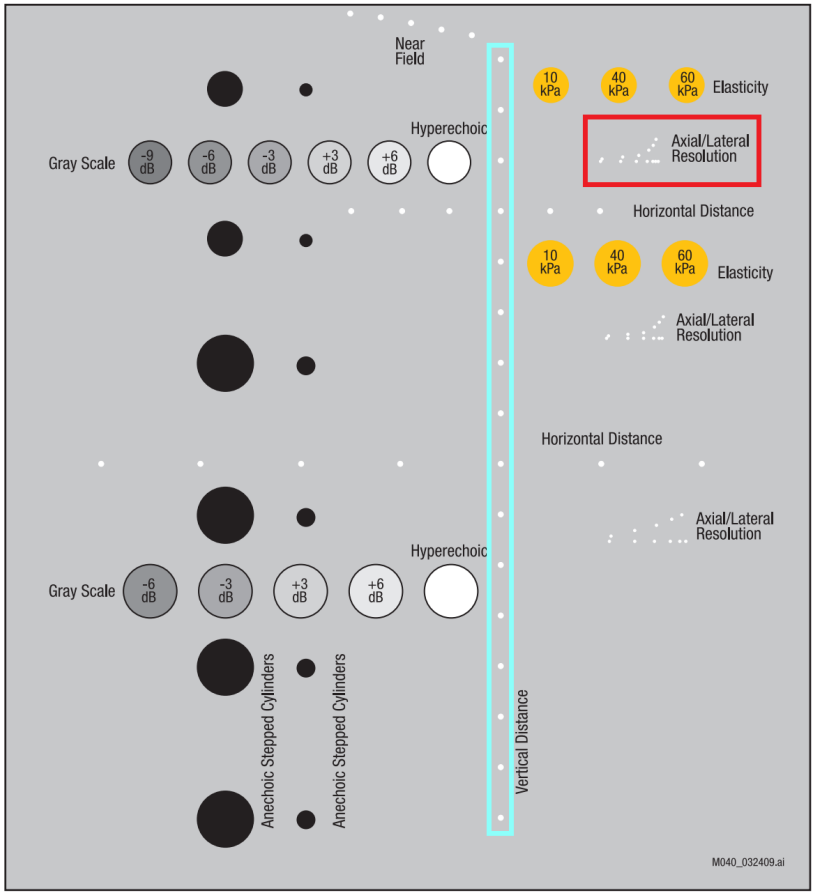

(b)

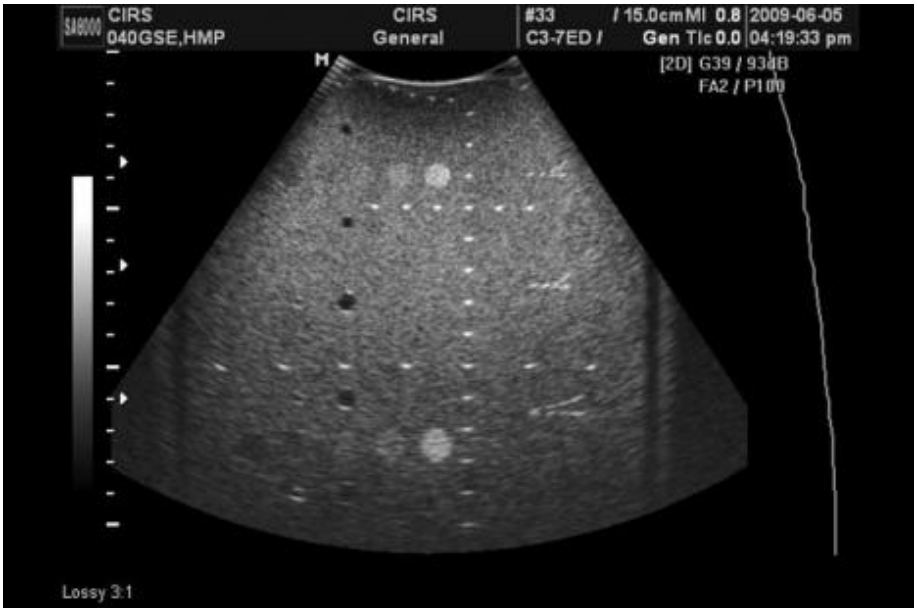

Figure 3.3: The inside of the CIRS 040GSE phantom. (a) Schematic. (b) An example of how it should look on a scan. Both images are taken from the specification manual of the phantom [11].

3.2.2 Data acquisition and processing

For data acquisition the Nyquist 200% bandwidth sampling setting of the Verasonics is used, which means that 4 samples per period are taken resulting in a sampling frequency of 10 MHz [12]. A region of -30 to 30 degrees will be divided into 500 scan lines for a proper resolution. The resulting data will then be processed in the same way as with the simulation, and the NSI constant will be chosen based on the simulation results.

Cross-sections will be made at the depths of the lateral resolution regions and at four evenly spaced line scatter targets to compare the NSI apodization technique to the rectangular one. Beside the beamwidth and MSR, also the speckle patterns will be compared between the two methods. This is done by using the signal to noise ratio (SNR) defined as the mean divided by the variance of the signal, equation 3.1. Both are measured in the region of interest, the region where the speckle is expected to be.

$$SNR = \frac{\langle |E| \rangle}{\sqrt{\langle |E|^2 \rangle - \langle |E| \rangle^2}} \tag{3.1}$$

where E is the signal strength. For a fully developed speckle the SNR is expected to be 1.91 [13]. This is done for the three apodization constants 0.05, 0.10 and 0.20.

Based on Reeg an improvement in beamwidth of 10 to 25 times, an improvement in MSR of 20 dB and an average NSI speckle SNR of 0.68 are expected.

To see the effect of NSI on tight spaced lateral scatter targets the lateral resolution region area of the CIRS phantom will be looked at quantitatively.

3.3 Possible problems

3.3.1 Undeveloped speckle

As shown by Reeg the speckle is expected to be greatly reduced when using the NSI method [1]. To overcome these problems two proposed solutions will be tried. In the first one the rectangular apodization image and the NSI apodization image are added together with weights of 50% to increase the speckle, the compounding technique. In the second one the NSI image is used as a colored overlay to the rectangular image to show how the method would work as an assisting tool for pointing out details.

3.3.2 Sampling issue with NSI

Another problem might occur because the NSI technique is heavily based on the sharp drop to zero in the middle. When the interval between scan lines is too big, it could theoretically happen that the sharp drop is skipped over. When subtracting the bridged image by the zero-mean apodization image this signal could fully vanish. This is illustrated in figure 3.4. To verify that this problem can occur, the same set-up is used as in the simulation but now one line scatter target is positioned slightly besides the middle axis, such that it gets partly skipped during scanning. The results will be shown as a transversal cross-section to show possible reductions in strength.

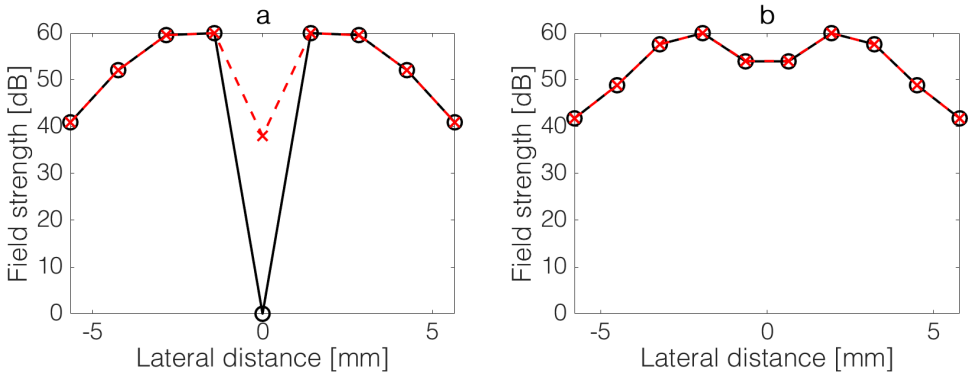

Figure 3.4: The dashed line represents the bridged image and the solid line represents the NSI image. (a) Illustrates proper line sampling. (b) Illustrates to low line sampling, notice that the sharp drop to zero in the middle is skipped.

4. Results

4.1 Simulation

The images resulting from the simulation, with c = 0.05 for the NSI apodization scheme, are shown in Figure 4.1. The cross-sections are taken at the depths of the line scatter targets and displayed in Figure 4.2. They are laterally cut of at -10 and 10 mm since that area is of most interest. The results gathered are shown in table 4.1. The results for c is 0.1 and 0.2 can be found in table 4.2 and 4.3, the corresponding cross sections of the radiation patterns can be found in Figure 4.3 and 4.4 respectively.

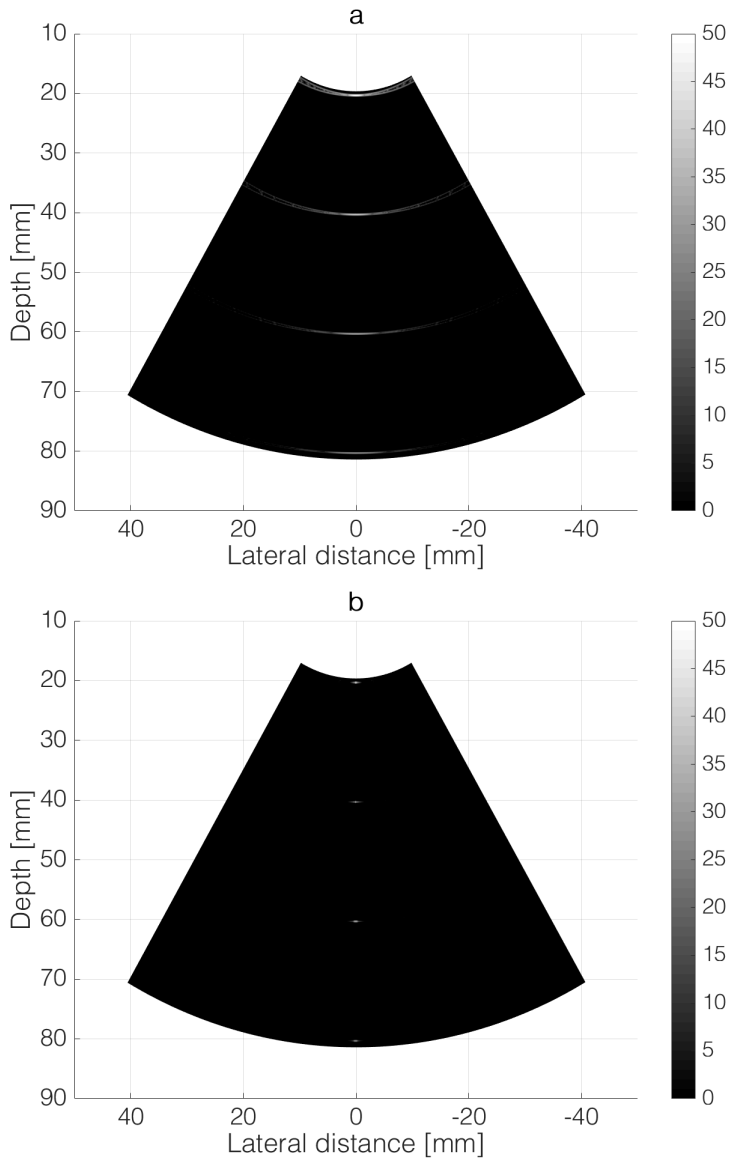

Figure 4.1: Phased array images made from virtual phantom with line scatterers at 20, 40, 60 and 80 mm at 50 dB dynamic range from -30 to 30 degrees. (a) Image made using rectangular apodization. (b) Image made using NSI apodization scheme.

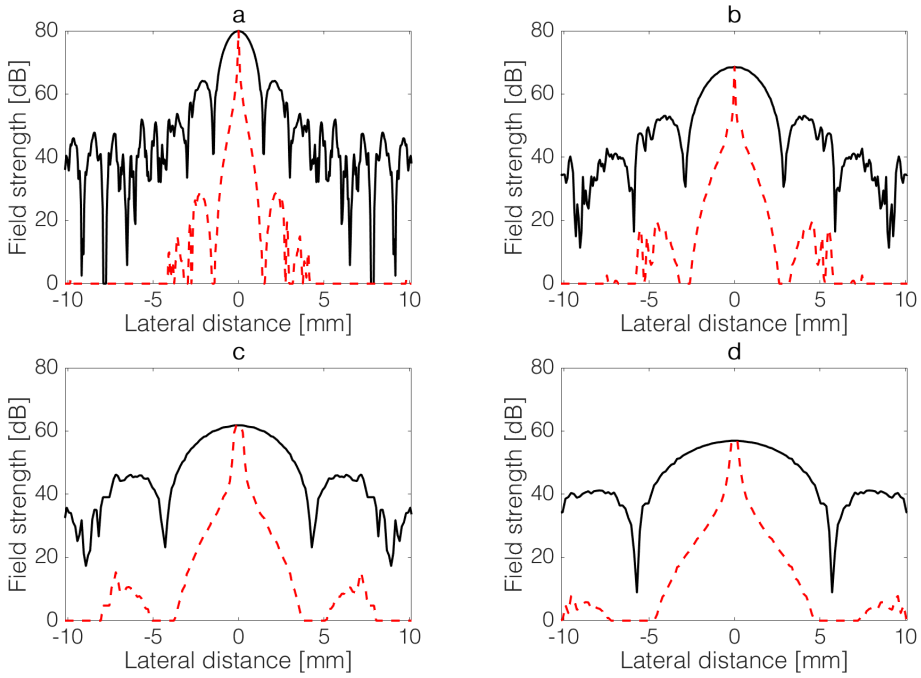

Figure 4.2: Cross-sections of figure 4.1 at respectively 20, 40, 60 and 80 mm depth, with a dynamic range of 80 dB. The solid line is the the image with rectangular apodization and the dashed line is made using the NSI apodization scheme with c = 0.05.

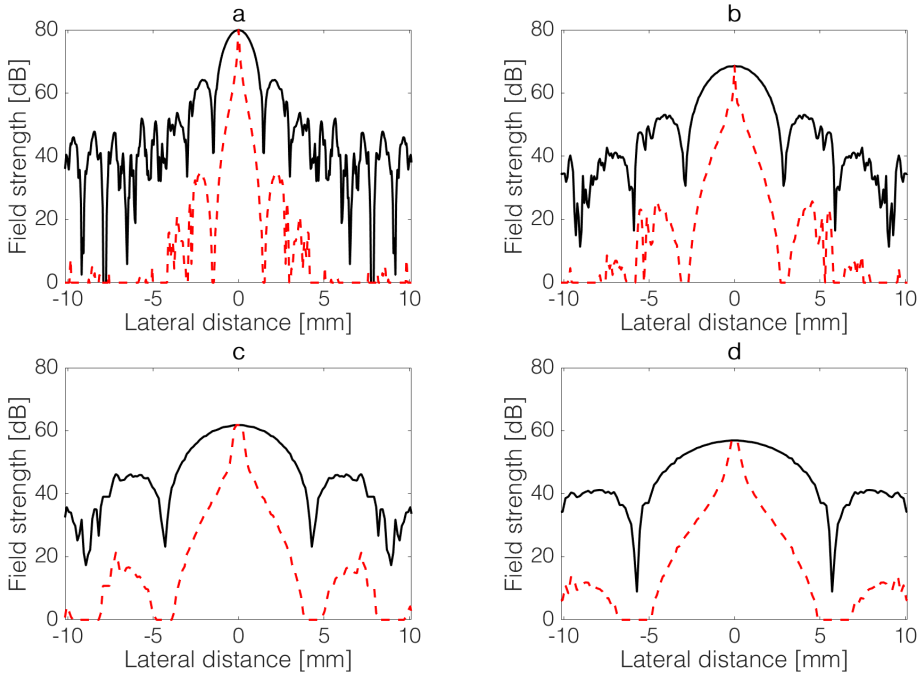

Figure 4.3: Cross-sections at respectively 20, 40, 60 and 80 mm depth, with a dynamic range of 80 dB. The solid line is the the image with rectangular apodization and the dashed line is made using the NSI apodization scheme with c = 0.1.

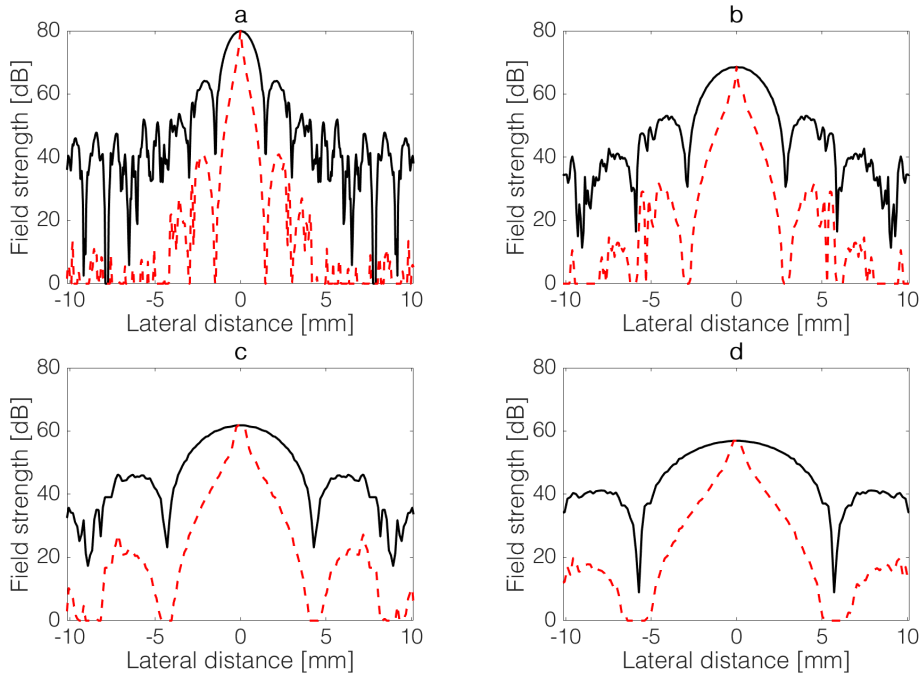

Figure 4.4: Cross-sections at respectively 20, 40, 60 and 80 mm depth, with a dynamic range of 80 dB. The solid line is the the image with rectangular apodization and the dashed line is made using the NSI apodization scheme with c = 0.2.

The results are as expected with large beamwidth and MSR improvements. Only at 60 mm, Figure 4.2c, it seems that an artefact of the method is present, as the top of the NSI image is rounded of. This could be due to the sampling issue discussed in chapter 3.3.2. Overall a constant of 0.05 leads to the highest reduction in beamwidth, on average 22.5 times, and increase in MSR of on average 33.4 dB.

Table 4.1: Simulation results estimated from cross-sections Figure 4.2 for c = 0.05. Expected beamwidth is calculated using formula 2.3.

	Beamwidth [mm]			**MSR [dB]**		**Improvement**	
Depth [mm]	Expected	Rect	NSI	Rect	NSI	Beamwidth	MSR [dB]
20	3.3	3.4	0.2	15.9	51.0	2128%	35.1
40	6.6	7.1	0.2	15.5	48.9	4604%	33.4
60	9.9	10.8	1.3	15.5	46.5	857%	31.0
80	13.2	14.0	1.0	15.6	49.8	1404%	34.2
Average				15.6	49.0	2248%	33.4

Table 4.2: Simulation results estimated from cross-sections Figure 4.3 for c = 0.1. Expected beamwidth is calculated using formula 2.3.

	Beamwidth [mm]			**MSR [dB]**		**Improvement**	
Depth [mm]	Expected	Rect	NSI	Rect	NSI	Beamwidth	MSR [dB]
20	3.3	3.4	0.2	15.9	45.2	1418%	29.3
40	6.6	7.1	0.3	15.5	44.1	2363%	28.6
60	9.9	10.8	1.5	15.5	40.5	720%	24.9
80	13.2	14.0	1.3	15.6	43.3	1045%	27.7
Average				15.6	43.3	1387%	27.6

Table 4.3: Simulation results estimated from cross-sections Figure 4.4 for c = 0.2. Expected beamwidth is calculated using formula 2.3.

	Beamwidth [mm]			**MSR [dB]**		**Improvement**	
Depth [mm]	Expected	Rect	NSI	Rect	NSI	Beamwidth	MSR [dB]
20	3.3	3.4	0.4	15.9	40.1	774%	24.2
40	6.6	7.1	0.5	15.5	36.9	1399%	21.4
60	9.9	10.8	1.8	15.5	34.5	600%	19.0
80	13.2	14.0	2.6	15.6	39.1	540%	23.5
Average				15.6	37.7	828%	22.0

4.2 Experiment

4.2.1 Line targets

First an image is made of the line scatter targets, for this an apodization constant, c, of 0.1 is used. This opposed to the 0.05 that came out best at the simulation. Using the later resulted in an artefact, where the bridged image had a lower peak than the zero mean apodization image. When subtracting these images this would lead a sudden drop for the NSI image where a sharp peek is expected. This effect is shown and highlighted in Figure 4.5.

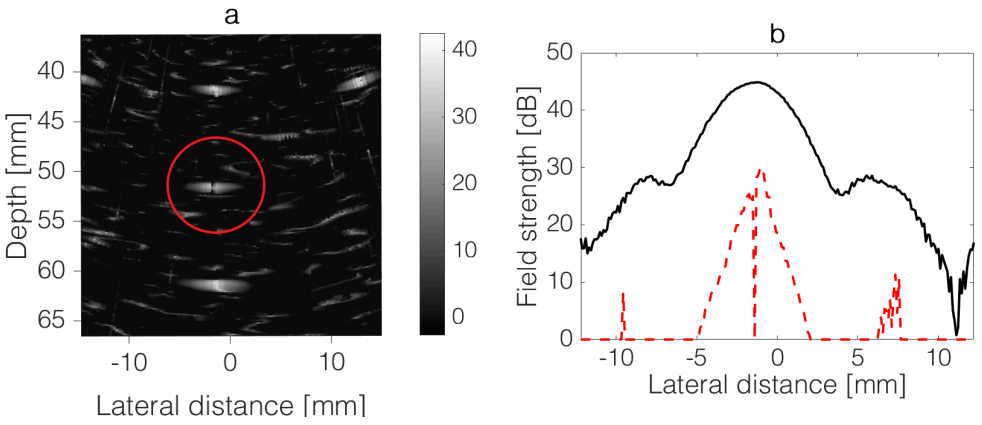

Figure 4.5: (a) A zoomed version of the c = 0.05 NSI image, the artefact is highlighted with the circle. (b) Cross-section at the depth of the highlighted artefact. The solid line is the rectangular apodization image and the dashed line is the NSI image. An unexpected loss in strength and a sudden drop in the NSI image can be seen.

The experimental images using an apodization constant of 0.1 are shown in Figure 4.6, the data up until the start of the far-field is set to zero. For the cross-sections the uneven four line scatter targets are chosen for an even distribution over the depth of 100 mm. This were respectively the line scatters located at a depth of 31.9, 51.5, 71.3 and 91.2 mm. These are shown in Figure 4.7, again with a constant lateral width on the axis. The MSR and beamwidth are estimated and displayed in table 4.4. The average MSR increase is 20.5 dB and the beamwidth reduces on average 5 times, which is lower than the values from the simulation. This and the artefact that is present when using c = 0.05 will be discussed later. From Figure 4.6 it can be seen that the highly echoic area that is also captured in the images is good visible when using the rectangular window apodization, while it is not recognizable as a circle in the NSI image.

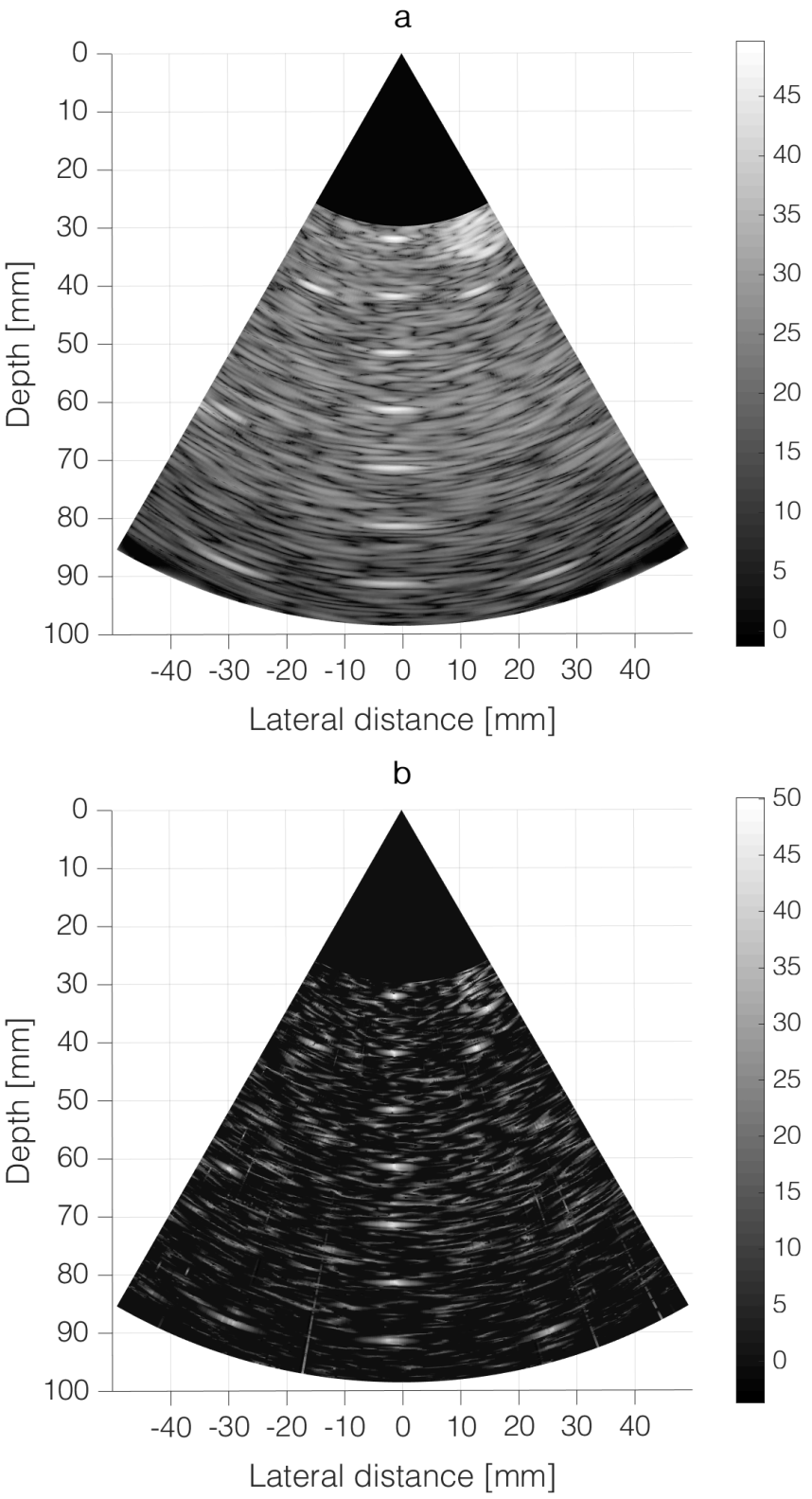

Figure 4.6: Phased array images made with P4-1 from CIRS phantoms line scatterer targets from -30 to 30 degrees. The dynamic range is 50 dB. (a) Image made using rectangular apodization. (b) Image made using NSI apodization scheme with c = 0.1.

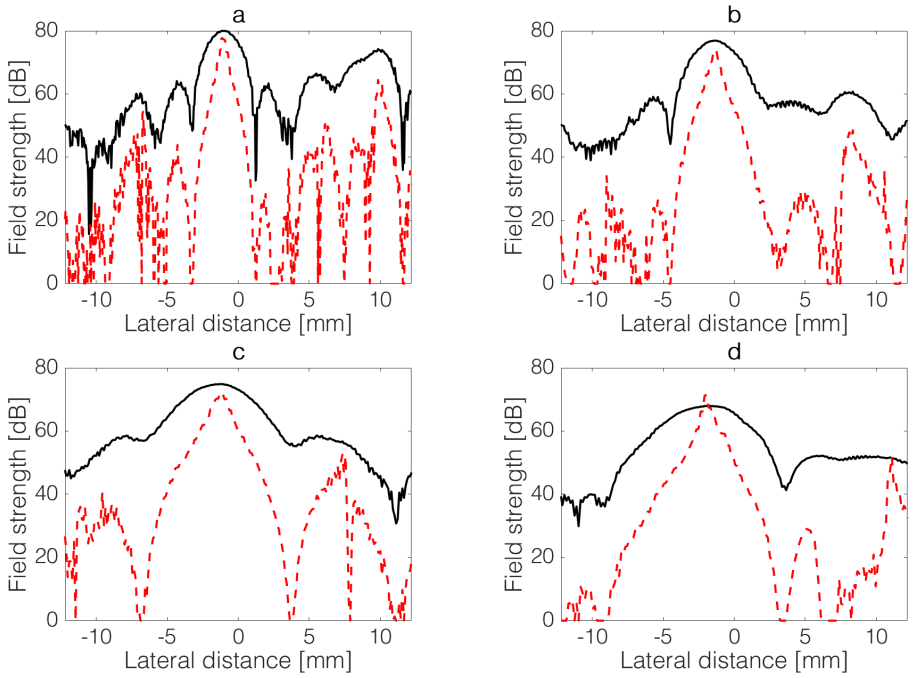

Figure 4.7: (a, b, c, d) Cross-sections at respectively 31.9, 51.5, 71.3 and 91.2 mm depth, with a dynamic range of 80 dB. The solid line is the image with rectangular apodization and the dashed line is made using the NSI apodization scheme with c = 0.1.

Table 4.4: Experimental results estimated from cross-sections shown in Figure 4.7 for c = 0.1. Expected beamwidth is calculated using formula 2.3.

	Beamwidth [mm]			**MSR [dB]**		**Improvement**	
Depth [mm]	Expected	Rect	NSI	Rect	NSI	Beamwidth	MSR [dB]
31.9	2.7	2.2	0.5	16.0	33.7	478%	17.7
51.5	4.3	3.6	0.8	17.7	47.6	469%	29.9
71.3	6.0	5.7	1.5	16.3	24.1	390%	7.8
91.2	7.7	6.0	0.9	15.8	42.6	667%	26.8
Average				16.5	37.0	501%	20.5

4.2.2 Lateral resolution targets

The lateral resolution targets are shown in Figure 4.8. In Figure 4.8e it can be seen that there are 7 lateral scatter targets of which 3 are tightly spaced. Using the rectangular apodization, Figure 4.8b, 5 lateral targets can be distinguished since the tightly spaced targets are seen as one. When the cross-section is taken, the solid line of Figure 4.8d, the middle target is not visible, this is due to the slight curvature of the line on which the targets lay in the image. When using the NSI apodization scheme with an apodization constant of 0.1, Figure 4.8c. The badly visible target from the cross-section vanishes and only 4 targets are distinguishable although, with a higher precision as shown in Figure 4.8d.

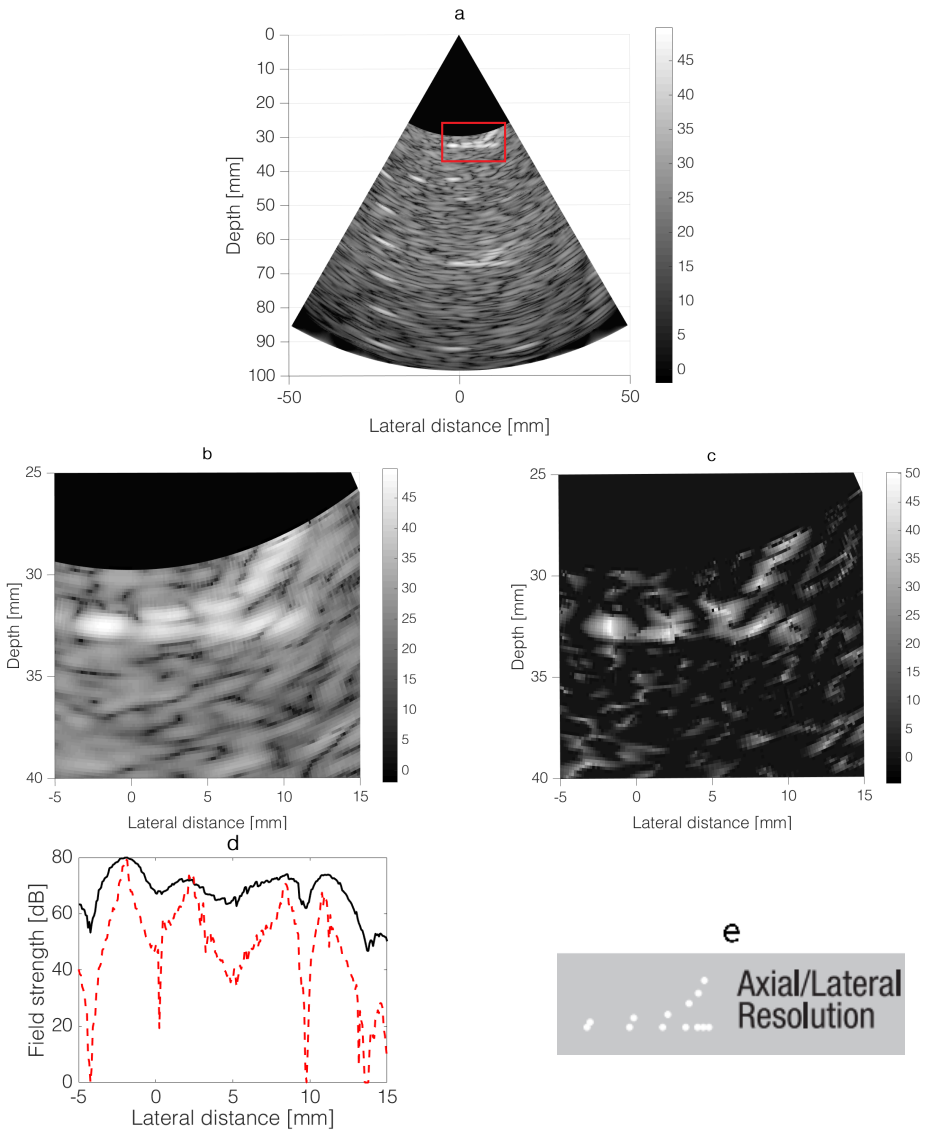

Figure 4.8: (a) Image of the lateral resolution targets of the phantom using a rectangular apodization with a dynamic range of 50 dB, the red box shows the closer inspected area. (b) Zoomed version of (a). (c) Corresponding NSI image with an apodization constant of 0.1. (d) A cross-section of the lateral resolution targets along the lateral axis with a dynamic range of 80 dB. The solid line corresponds to b and the dashed line to c. (e) Schematic expectation for b and c [11].

4.2.3 Speckle

As could be already seen in Figure 4.6 speckle seems to get reduced. To quantify this reduction the SNR of an area only consisting of speckle is determined using formula 3.1. The area chosen can be seen in Figure 4.9 with the corresponding results in table 4.5. The image using the rectangular window apodization shows a value near the expected of 1.91. The SNR is lower for the NSI images, suggesting undeveloped speckle, and seems to scale with the apodization constant i.e. with energy. Apart from a lower SNR the speckle also gets more point like when using the NSI apodization scheme.

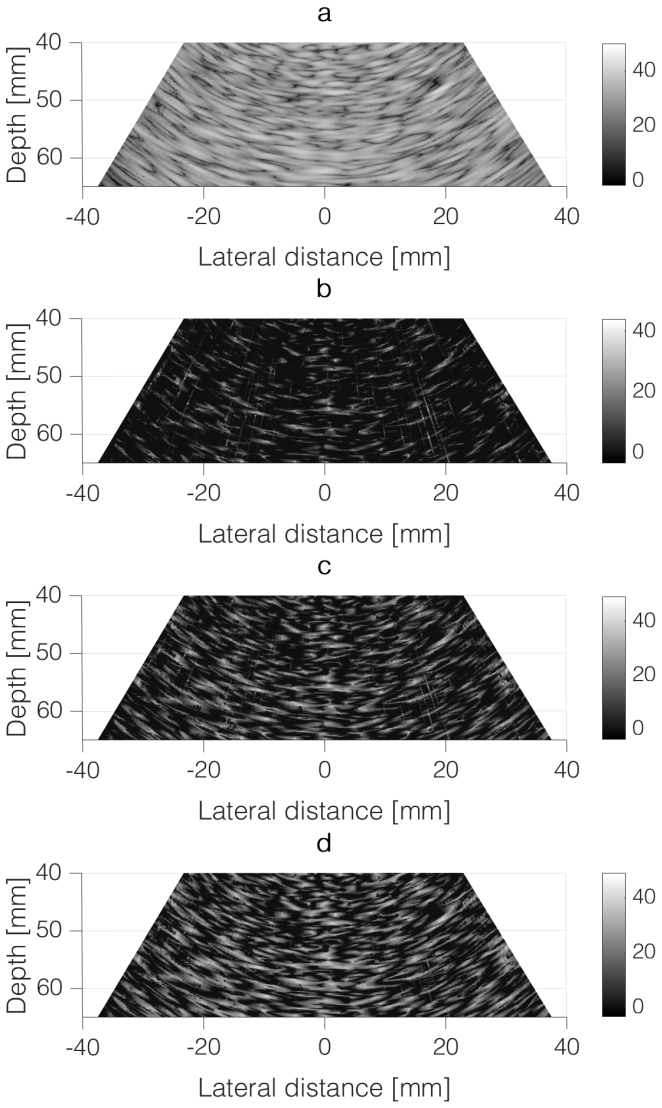

Figure 4.9: Area chosen to do the SNR measurement of speckle, all shown with 50 dB dynamic range. (a) The rectangular apodization image. (b, c, d) The NSI images using an apodization constant of respectively 0.05, 0.1 and 0.2.

Table 4.5: Results of speckle SNR for area corresponding to Figure 4.9.

	Rect	**NSI**		
		c = 0.05	c = 0.1	c = 0.2
SNR	1.78	0.35	0.52	0.64

4.3 Possible problems

4.3.1 Dealing with undeveloped speckle

To overcome the reduction in speckle two possible applications of the technique are looked at. First, compounding to combine the NSI and rectangular apodization images into one and second, overlaying to act as an assisting tool to spot small scatter targets.

Compounding

Figure 4.6a and 4.6b are combined into Figure 4.10, both with a 50% weight. The highly echoic area is better visible compared to the NSI image while line scatter target still have a sharper center than in the rectangular apodization image. The cross-sections are shown in Figure 4.11 and the results in table 4.6. The speckle SNR for the compounded image is calculated to be 1.71.

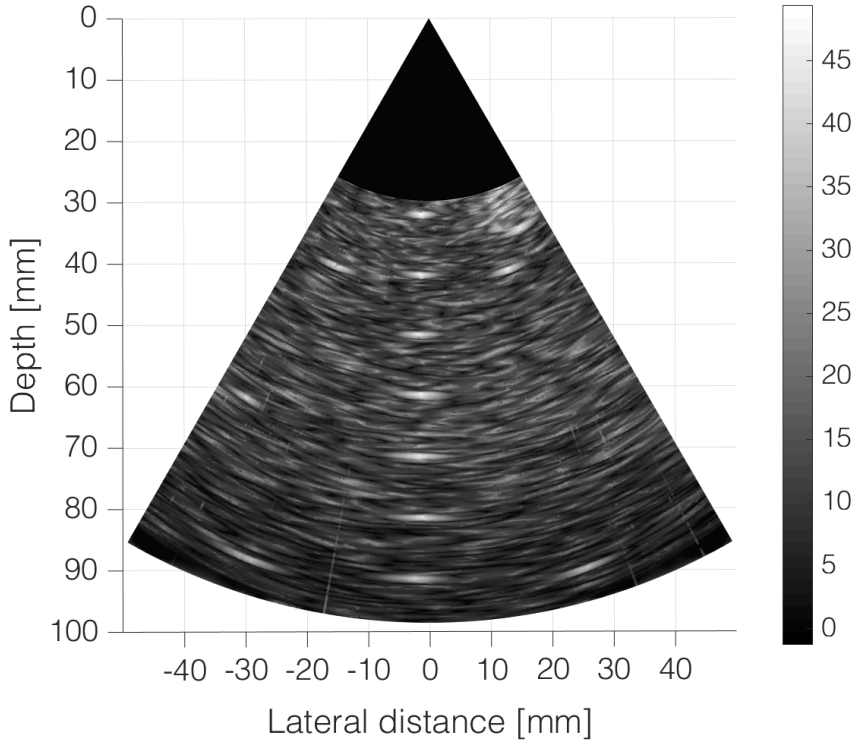

Figure 4.10: Compounded image using a 50% weight for both the rectangular apodization image and NSI image.

Table 4.6: Results of compounding (Comp) technique estimated from Figure 4.11. Previous results when using rectangular apodization and NSI are included for comparison.

	Beamwidth [mm]			**MSR [dB]**		
Depth [mm]	Rect	NSI	Comp	Rect	NSI	Comp
31.9	2.2	0.5	1.5	16.0	33.7	20.7
51.5	3.6	0.8	2.0	17.7	47.6	23.1
71.3	5.7	1.5	3.4	16.3	24.1	22.1
91.2	6.0	0.9	2.5	15.8	42.6	23.5
Average				16.5	37.0	19.9

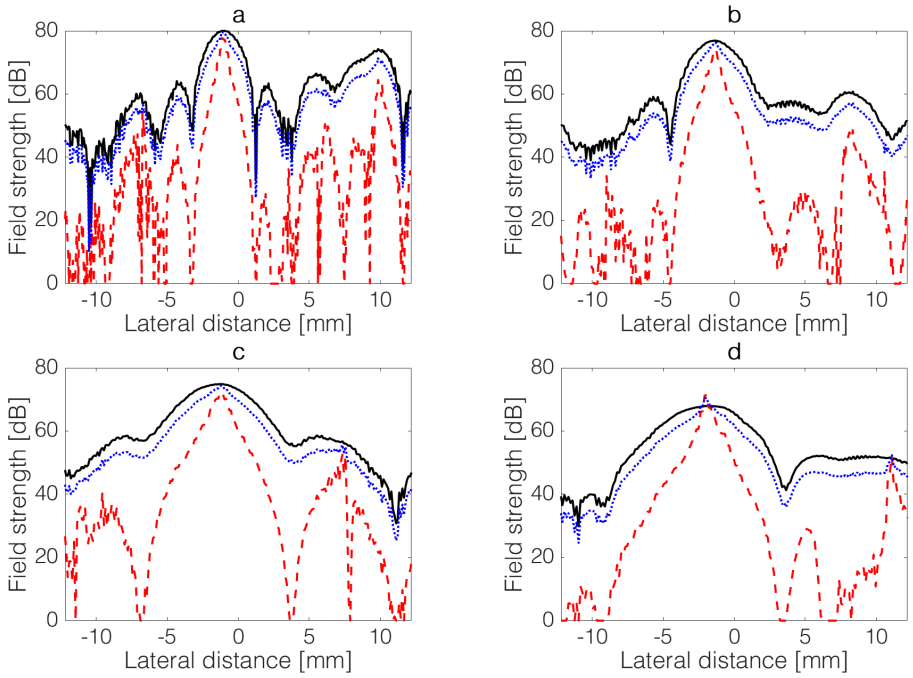

Figure 4.11: (a, b, c, d) Cross-sections at respectively 31.9, 51.5, 71.3 and 91.2 mm depth, with a dynamic range of 80 dB. The solid line is the the image with rectangular apodization, the dashed line is made using the NSI apodization scheme with c = 0.1 and the dotted line is the radiation pattern of the compounded image.

Overlay

The result of using the NSI image as an overlay for the rectangular apodization image is shown in Figure 4.12. This method is shown for the lateral resolution scatter targets since this is where extra distinguishing between targets could be useful.

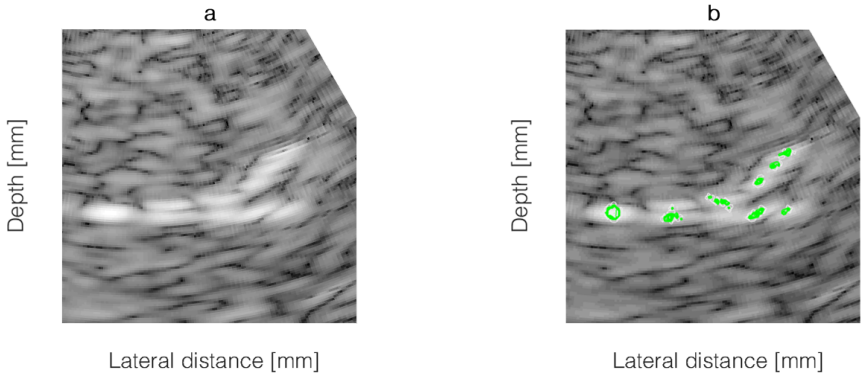

Figure 4.12: (a) Reference image using rectangular apodization. (b) Overlay image where the highest 10 dB of the NSI image is plotted in green on top of the rectangular apodization image.

4.3.2 Sampling issue with NSI

For this simulation the apodization constant of 0.05 is used, the same area from -30 to 30 degrees and artificial phantom as during the simulation are scanned but now using only 100 scan lines opposed to 500. Using this resolution interval the x-coordinate between two line acquisitions can be calculated as follows:

$$x_{scat2} = \frac{40}{1000} \cdot sin(60°/100)/2 = 2.0944 \cdot 10^{-4} \tag{4.1}$$

the first term comes from the depth of the line scatter target (40 mm), sin since we want the x displacement, $\frac{60°}{100}$ to move one sample and dividing by 2 to be in between the samples.

The second line scatter target is chosen to be displaced since the first one is used for normalizing both images. The displacement is chosen such that the line scatter target falls exactly in between the lateral samples. The results of this worst case scenario are shown in Figure 4.13. As expected all but the second line scatter target are effected. The suppression is around 20 dB which is significant considering that the total amplitude is only 50 dB that in the ideal situation. Although the signal of the second scatter is suppressed, taking a lateral cross section shows that the relative sharpness opposed to the original image stays, see Figure 4.14, only the sharp peak is less present.

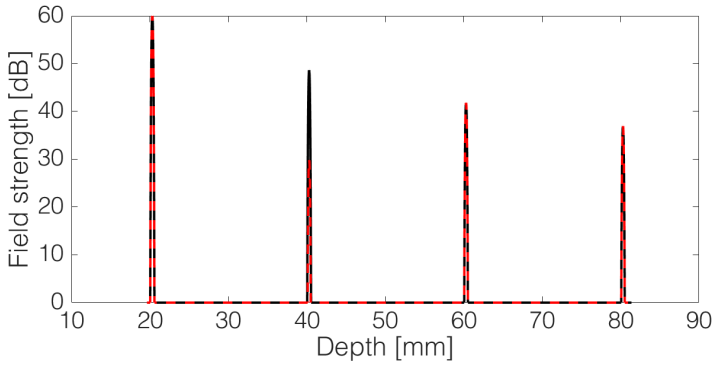

Figure 4.13: Transversal cross-section through the line scatter targets. The solid line (black) represents the image taken with perfect lateral sampling. The dashed line (red) represents the image where the second scatterer at 40 mm depth has worst case lateral sampling.

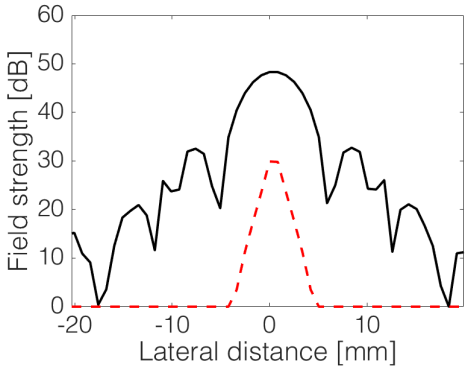

Figure 4.14: Lateral cross-section at a depth of 40 mm. The solid line represents the original image. The dashed line represents the NSI image.

5. Discussion

The simulation results are as expected. The beamwidth using a rectangular apodization follows formula 2.3. Also, an on average 22.5 time reduction in beamwidth and 33.4 dB higher MSR for the NSI technique when using an apodization constant of 0.05 is achieved opposed to using a rectangular apodization. These are in agreement with the findings of Reeg. Unexpected is the NSI beamwidth of the third line scatter target (60 mm depth). Namely in two of the three cases the NSI beamwidth is higher than that of the fourth line scatter target (80 mm depth). A contributing factor could be the improper line sampling as discussed in chapter 3.3.2, for 500 lines over 60° at a depth of 60 mm which results in a lateral interval of 0.1 mm.

Besides improper lateral sampling something else can occur. When focussing on an area the delay times are calculated accordingly (formula 2.1) to perform DAS. When these calculated delay times are transformed to integer matrix elements, the form in which the data is stored, rounding errors are made since these transformed times are almost never going to be an exact integer. This can lead to improper summation, because actually some data is from behind the focus point and some data from in front of it (see Figure A.2 in the appendix for an illustration). For the NSI method this means that in some cases the zero-mean apodization image does not have a sharp drop to zero in the middle which upon subtraction from the bridged apodization image does not turn into a sharp peak.

That this occurs for the simulation can be confirmed since doubling the sampling frequency to 200 MHz eliminates the rounded peak reducing the beamwidth to 0.26 mm for the third line scatter target at a depth of 60 mm as shown in Figure 5.1.

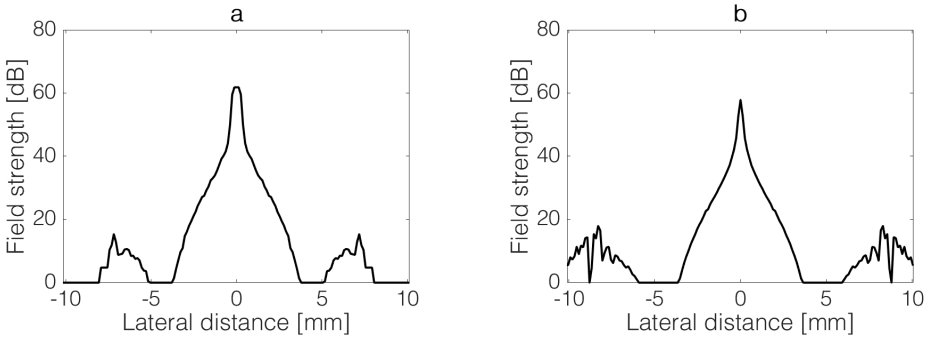

Figure 5.1: Cross-section of NSI image of simulation using line scatter targets at a depth of 60 mm. (a) Using a sampling frequency of 100 MHz resulting in a beamwidth of 1.3 mm. (b) Using a sampling frequency of 200 MHz resulting in a beamwidth of 0.26 mm.

The experimental results for the line scatter targets were less than expected and started of with showing an artefact for an apodization constant of c = 0.05. This is probably again due to the integer rounding of the delays and is confirmed by choosing a point which shows this artefact. Here the rounding led to the bridging image being lower then the zero-mean image at the point where the artefact shows. To confirm this the round function (rounding to the nearest integer) is changed to the floor function (rounding to the nearest integer towards minus infinity) in MATLAB resulting in Figure 5.2. Here a clear difference can be seen.

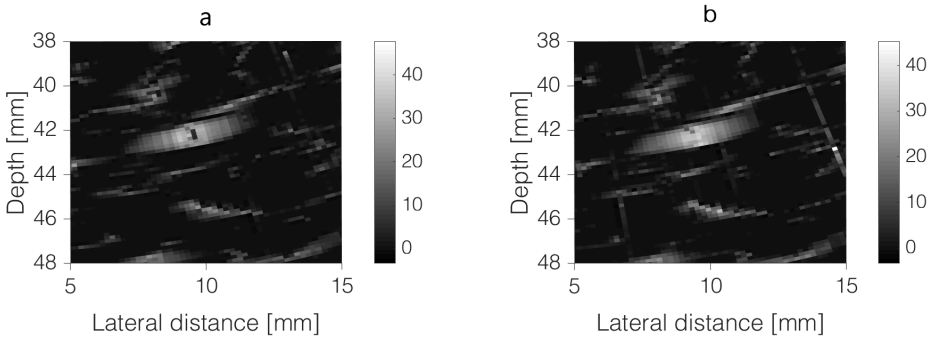

Figure 5.2: Images using NSI with an apodization constant of 0.05. (a) For this image the function round is used for the time delay rounding. (b) For this image the function floor is used for the time delay rounding.

The artefact problem was solved by using a higher apodization constant since that increases the distance between the 'bridge' and the 'zero'. Making that the bridging image becomes higher then the zero-mean image at that particular point, as it always should be. Besides the artefact problem, almost no sharp peaks where measured, which is probably also due to the effect of rounding that is occurring for almost every measurement as there are only 4 samples per wavelength. Assuming a worst case rounding error this could lead to an error in phase of $\frac{\pi}{2}$ (rounding up half an integer results in $\frac{\pi}{4}$, so does rounding down) before summation. This could lead to data adding up instead of cancelling out. The line scatter target at 91.2 mm depth seems sampled well relative to the others since a sharp peak is present.

The MSR is increased by 20.5 dB, again in accordance with the findings of Reeg. This is as expected since the MSR should not be affected in a significant way by the before mentioned problems. The difference in beamwidth for the rectangular apodization versus the expectation could be due to the assumed speed of sound in tissue of 1540 m/s. Furthermore, other imperfections in the CIRS phantom could play a role since some of the cross-sections do not seem te be symmetric around the top.

The experimental results for the lateral scatter targets show a similar reduction in beamwidth to the line scatter targets when taking the cross-section. Unfortunately, the three tightly spaced scatter targets are not revealed when using the NSI method. To make a conclusive statement about this, first the sampling issues have to be resolved.

The experimental results for the SNR of the speckle are in agreement with literature. It seems that the speckle scales with the energy in an image. For NSI this energy scales in some way with the apodization constant. To overcome the reduction in speckle two methods were proposed, compounding and overlaying. Compounding brings the SNR back to 1.71 while keeping a reduction in beamwidth. For the point at 91.2 mm depth it can be seen that the sharp peak carries over to the compounded image. Since the other peaks were not sharp, better results are expected when having proper sampling. A disadvantage of compounding seems to be that side lobe levels almost do not improve as opposed to the rectangular apodization. The overlay method shows that NSI could be used as an addition to traditional imaging in pointing out hard-to-spot scatter targets.

To solve the rounding sampling issue two things can be done. First, the sampling frequency could be set higher since as a result the error in rounding becomes smaller. However, as shown in the simulation this would not be a perfect solution, since having a sampling frequency of 100 MHz for a 7.5 MHz signal still showed artefacts. An other way would be to use a more advanced way of delaying where interpolation or something similar could be used when array elements do not align perfectly.

In simulation also the lateral sampling issue is shown to exist. For both sampling issues, rounding and lateral, further studies are needed to measure the precise effect on NSI and determine minimum specifications for this technique to work properly. Furthermore, studies can also be done for solving the speckle problem and understanding better how it behaves. The compounding and overlaying method could be investigated further and new methods could be proposed.

After this is understood the technique can be implemented for three dimensional imaging with possibly a beamwidth reduction along both lateral axes of 25 times and high side lobe reduction. So far it seems that six images are needed to make the method work. This is explained further in Apendix A.4.

As a last point, one might argue that the NSI image can be made from the rectangular apodization image by putting the threshold higher, since there is more energy in the rectangular apodization image as opposed to the NSI image. To show this is not correct, the field strength is measured in both the rectangular apodization image and the NSI image, and the threshold is changed accordingly. It was found that there was an even amount of energy in both images when putting the rectangular apodization image threshold at 42.5 dB and the NSI image threshold at 20 dB, see Figure 5.3. It can be seen that a lot of scatter targets vanish from the rectangular apodization image compared to the NSI image.

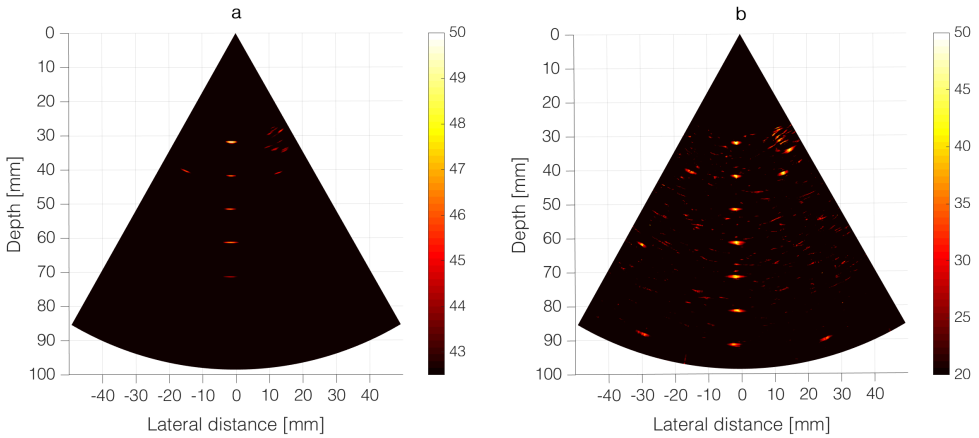

Figure 5.3: Comparison between rectangular apodization image (a) and NSI image (b) when the threshold for the rectangular apodization image is set to 42.5 dB and to 20 dB for the NSI image. A different colormap than grey is used for improved visibility.

6. Conclusion

Overall it is shown that the Null Subtraction Imaging proposed by Reeg for linear transducers also works for phased array transducers. In the simulation the beamwidth is reduced by on average 22.5 times and MSR is on average 33.4 dB higher. Some artefacts were shown which could be due to lateral sampling. These results were achieved using an apodization constant of 0.05 and are in accordance with prevailing literature.

For the experiment an apodization constant of 0.1 was used resulting in an on average reduction in beamwidth of 5 times and an on average 20.5 dB higher MSR. The beamwidth reduction is lower than expected, probably due to rounding errors introduced by the integer element delays used in DAS. This could be resolved by using a higher sampling frequency or by using a more advanced delay algorithm where interpolation, or a similar technique, is used when delay times do not correspond to integer elements. The higher MSR was as expected.

When looking at tightly spaced lateral scatter targets the technique does not seem to reveal targets unseen by regular imaging. Although it still makes the scatter targets that where already present in the reference image better visible.

The speckle SNR for the rectangular apodization image, 1.78, is close to the expected 1.91, indicating fully developed speckle. While the NSI SNR speckle for apodization constants of 0.05, 0.1 and 0.2 were respectively 0.35, 0.52 and 0.64. These values are also close to the expected average of 0.68. The values seem to indicate that speckle scales with the energy present in the field.

The proposed solutions to undeveloped speckle, namely compounding and overlaying, seem to work. Where compounding shows reduced beamwidth over the rectangular apodization image with the disadvantage that side lobes are barely suppressed. Overlaying shows that the technique could act as an assisting tool to spot tightspaced scatter targets.

Further study on the NSI technique is needed to understand under what conditions this technique works properly. For this the lateral and rounding sampling issues need to be investigated further. Also the effect on speckle that NSI has could be investigated further, and possibly other hybrid solutions between NSI and an existing technique could be thought of. After this is understood and results are as expected, the next step would be to implement NSI into 3D imaging where possibly before-mentioned improvements on both lateral axes could be realised.

Bibliography

[1] J. R. Reeg. Null subtraction imaging technique for biomedical ultrasound imaging. Master's thesis, University of Illinois.

[2] J.A. Jensen and N. B. Svendsen. Calculation of pressure fields from arbitrarily shaped, apodized, and excited ultrasound transducers. *IEEE Trans. Ultrason., Ferroelec., Freq. Contr.*, 39:262–267, 1992.

[3] J.A. Jensen. Field: A Program for Simulating Ultrasound Systems. *Medical, Biological Engineering and Computing*, 34:351–353, 1996.

[4] M.A.P. Pertijs, J.G. Bosch, M.D. Verweij, and N. De Jong. 3D intra-cardiac echography: smart matrix transducer at the tip of a catheter. Project proposal.

[5] M. L. Oelze (Champaign IL US) and J. R. Reeg (Urbana IL US). Method and apparatus for null substraction ultrasound imaging. http://www.freepatentsonline.com/y2017/0108584.html, April 2017. Patent. US 20170108584.

[6] Thomas L. Szabo. *Diagnostic Ultrasound Imaging: Inside Out*. First edition, 2004.

[7] J. Kortbek, J.A. Jensen, and K. L. Gammelmark. Sequential beamforming for synthetic aperture imaging. *Ultrasonics*, 53(1):1 – 16, 2013.

[8] MathWorks. Envelope Detection. `https://nl.mathworks.com/help/dsp/examples/envelope-detection.html`. Accessed: 16-06-2017.

[9] J. Huijssen. *Modeling of Nonlinear Medical Diagnostic Ultrasound*. PhD thesis, Delft University of Technology.

[10] J.A. Jensen. Users' manual for the Field II program, 2011.

[11] Multi-Purpose, Multi-Tissue Ultrasound Phantom: Model 040GSE, 2013. Specification manual, CIRS Inc.

[12] Vantage Sequence Programming Manual, 2016. Verasonics Inc.

[13] B. S. Carmo, R. W. Prager, A. H. Gee, and L. H. Berman. Speckle detection for 3d ultrasound. *Ultrasonics*, 40(1):129 – 132, 2002.

A. Appendix

A.1 Fourier transforms

The Fourier transform of two rectangular functions multiplied, f_{rect}, is:

$$\mathcal{F}(f_{rect}) = A \cdot sinc(\frac{x}{\lambda z} N \cdot w) \tag{A.1}$$

where A is a certain constant, x is the lateral distance, N is the number of transducer elements, w the width of a transducer element, λ the wavelength and z the depth.
The Fourier transform of the zero-mean apodization function, f_{zm}, is:

$$\mathcal{F}(f_{zm}) = A \cdot \frac{\cos(\frac{\pi x}{\lambda z} N \cdot w) - 1}{x} \tag{A.2}$$

A.2 Data processing procedure

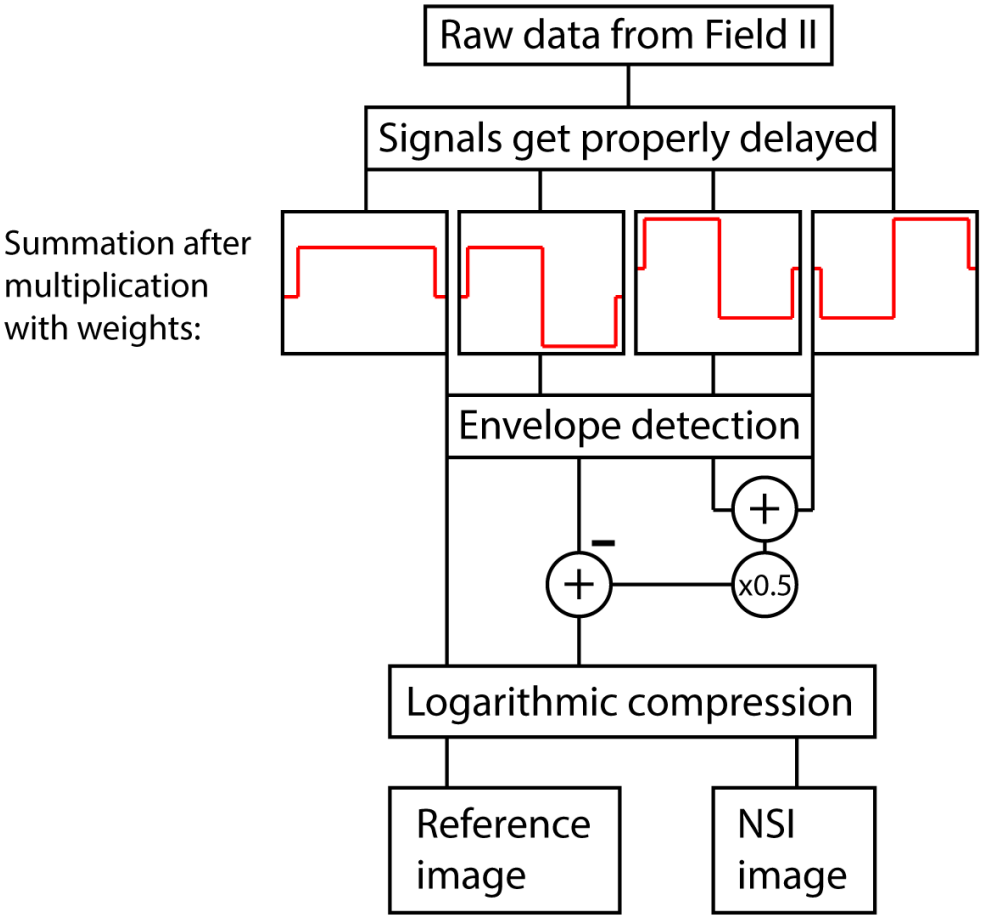

Figure A.1: Schematic of the data processing procedure from top to bottom.

A.3 Improper sampling illustration

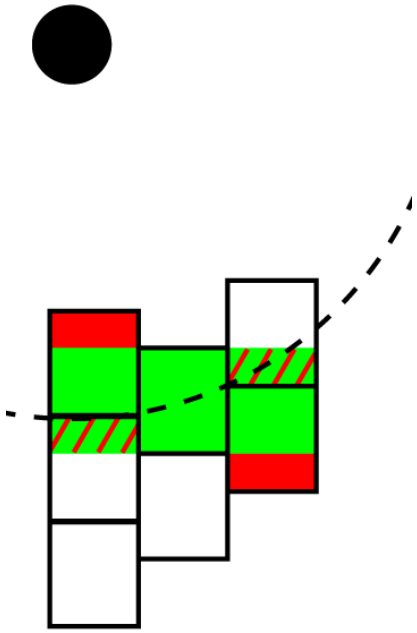

Figure A.2: An illustration of the improper sampling that can occur due to rounding errors. The dot is the point at which is focussed, the array elements are shifted accordingly. The proper data for the point is highlighted in green (light), due to the integer rounding error actually the red area (dark) is summed and part of the green area falls away (this is shown with red stripes trough the area). In this example this makes that for the left array you look to far away and for the right array you look to nearby.

A.4 Suggestions for 3D imaging

For implementing the NSI technique in 3D imaging an apodization scheme needs to be found for which the 2D Fourier transform has a sharp drop to zero in the middle, since for 3D imaging a 2D traducer is needed. From now on the x and y axis will form the plane in which the 2D traducer lays, and the z axis is the depth.

Applying the zero-mean apodization to both the x and y axis results in the following total apodization as can be seen in Figure A.3a with the corresponding Fourier transform in Figure A.3b. As can be seen in the image, a zero is present at the center but the drop of around it is slow compared to the four other zeros in the center (the square which contains the center four 'main' lobes) that all lay between two 'main' lobes.

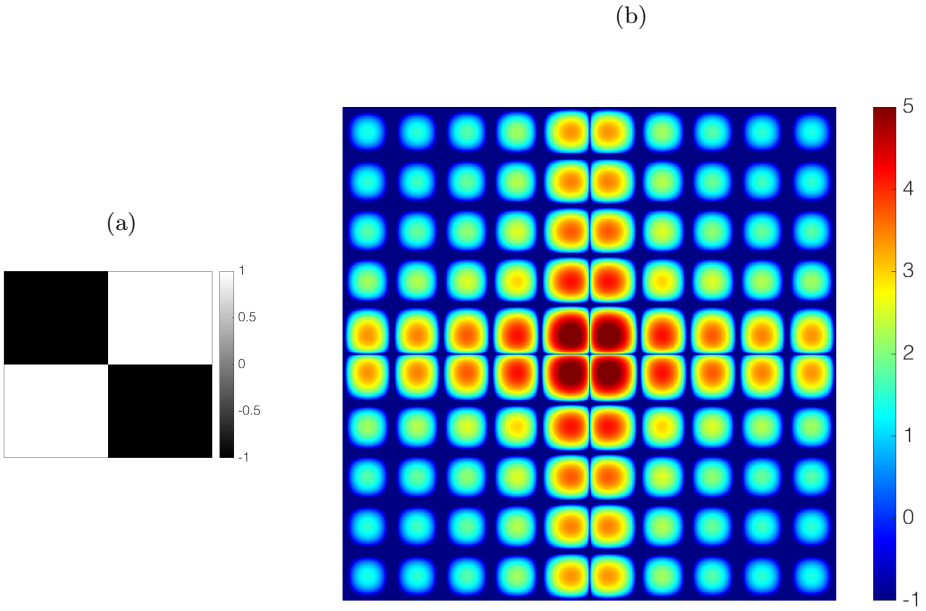

Figure A.3: (a) 2D zero-mean apodization that forms an extension of the 1D method. (b) Corresponding absolute Fourier transform to (a).

Using an apodization like in Figure A.4a and A.4c results in sharp zeros in the center as can be seen in the Fourier transform images of Figure A.4. This can be exploited by adding both Fourier transforms up to form Figure A.5. This results in a sharp zero in the middle, this zero is compared to another one in the center square in figure A.6. From this it can be seen that the central zero has the sharpest drop off.

Apart from making two zero mean images, each needs its own bridged image to work, so in total 6 (2 zero mean images and 4 images needed for bridging) apodizations need to be used. In my testing it seems that bridging works in the same was as it did for the 2D image. When the bridging image is made the zero-mean image can be subtracted to form the NSI image.

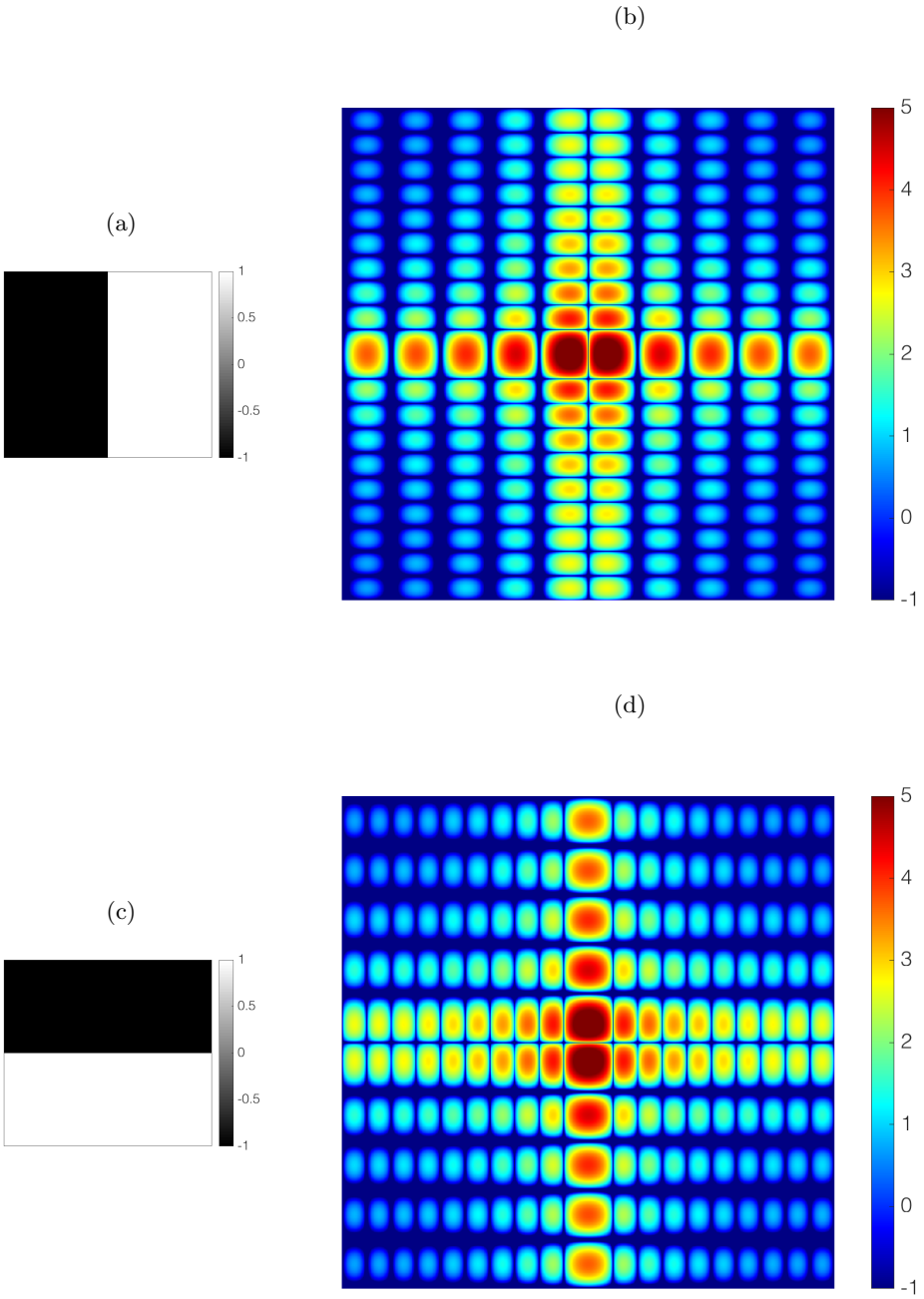

Figure A.4: (a) Apodization of 2D array. (b) Corresponding absolute Fourier transform to (a) with sharp drop to zero in the middle. (c) Apodization of 2D array. (d) Corresponding absolute Fourier transform to (c) again with sharp drop to zero in the middle.

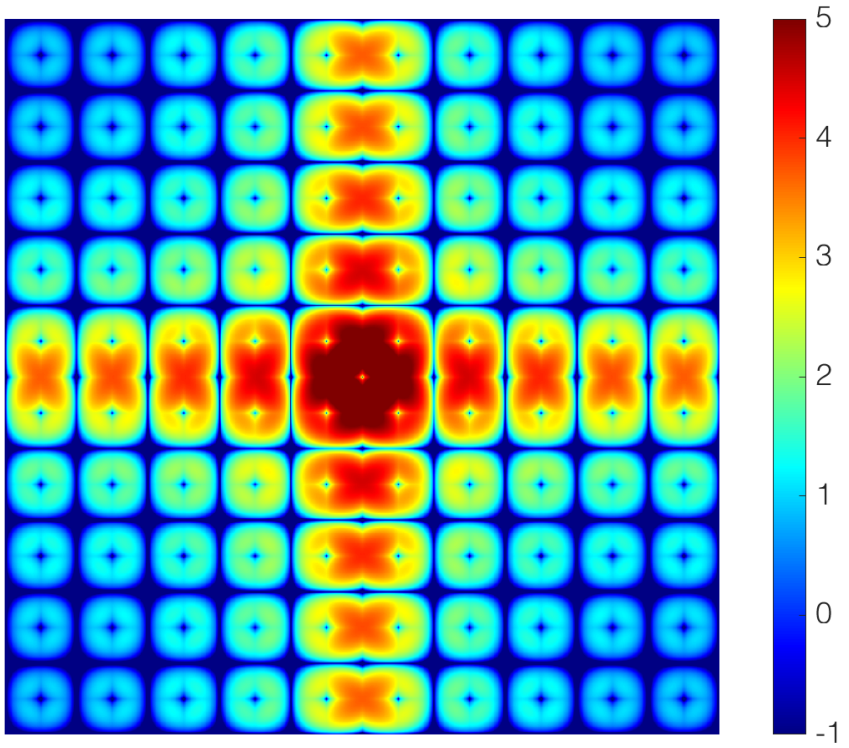

Figure A.5: Addition of the absolute Fourier transforms of Figure A.4b and A.4d.

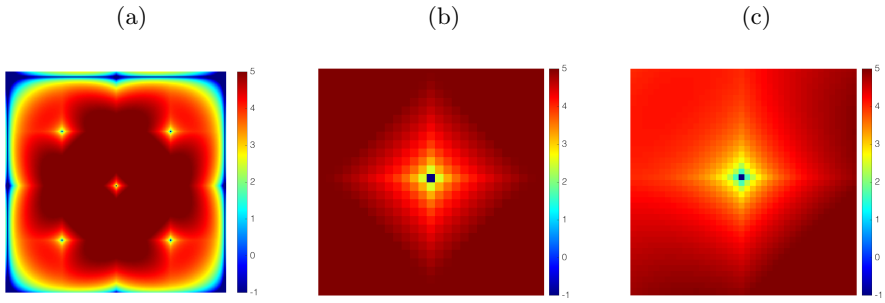

Figure A.6: Zoomed version of Figure A.5. (a) Zoom at center of Figure A.5. (b) zoom at central zero. (c) Zoom at top left zero.